



Multivariate Likelihood Search for Single-Top-Quark Production with 1.5 fb^{-1}

The CDF Collaboration
URL <http://www-cdf.fnal.gov>
(Dated: August 16, 2007)

We report results from the multivariate likelihood function search for single-top production with CDF II data corresponding to 1.5 fb^{-1} of integrated luminosity. Our expected median p -value is 2.0×10^{-3} (or 2.9σ), while the measured p -value is 3.1×10^{-3} , which corresponds to a 2.7σ excess over the Standard Model background (assuming $M_{top}=175 \text{ GeV}$). The best-fit value for the combined $s+t$ -channel production of single-top quarks assuming the Standard Model ratio of their production cross sections is $\sigma_s + \sigma_t = 2.7_{-1.1}^{+1.3} \text{ pb}$. Separately, the s -channel and t -channel cross sections fits are $1.1_{-1.1}^{+1.4} \text{ pb}$ and $1.3_{-1.0}^{+1.2} \text{ pb}$.

Preliminary Results for Summer 2007 Conferences

I. INTRODUCTION

According to the Standard Model, in $p\bar{p}$ collisions at the Tevatron top quarks can be created in pairs via the strong force, or singly via the electroweak interaction. The latter production mode is referred to as “single-top-quark” production and takes place mainly through the s - or t - channel exchange of a W boson (Figure 1). Both the CDF and DØ collaborations have reported single-top results using $\sqrt{s} = 1.96$ with approx. 1fb^{-1} of data, and the DØ collaboration has published 3σ evidence for single-top[13, 14].

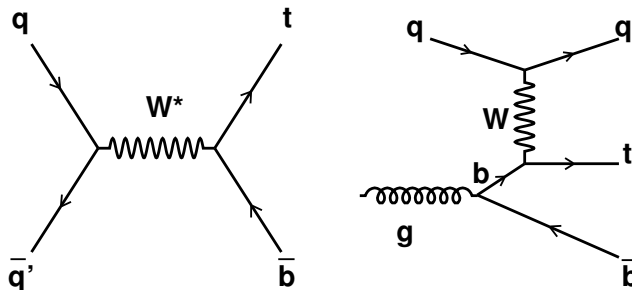


FIG. 1: Representative Feynman diagrams for single-top-quark production at the Tevatron: s -channel W^* (left) and t -channel W -gluon fusion (right).

Studying single-top production at hadron colliders is important for a number of reasons. First, it provides the only window into measuring the CKM matrix element $|V_{tb}|^2$, which in turn is closely tied to the number of quark generations. Second, measuring the spin polarization of single-top quarks can be used to test the V-A structure of the top weak charged current interaction. Third, single-top events represent an irreducible background to several searches for SM or non-SM signals, for example Higgs boson searches. Fourth and last, the presence of various new SM and non-SM phenomena may be inferred by observing deviations from the predicted rate of the single-top signal.

The theoretical single-top production cross section is $\sigma_{s+t} = 2.9$ pb for a top mass of 175 GeV/ c^2 [3]. Despite this small rate, the main obstacle in finding single-top is in fact the large associated background. After all selection requirements are imposed, the signal to background ratio is close to 1/10. This challenging, background-dominated dataset is the main motivation for using multivariate techniques. The following sections present the event selection, the signal and background estimations, an extended b -tagger and a kinematic solver used to improve signal identification, the statistical techniques, the expected and observed single-top cross section results, and a brief summary of these results.

II. SELECTION REQUIREMENTS

Our selection exploits the kinematic features of the signal final state, which contains a top quark, a bottom quark, and possibly additional light quark jets. To reduce multijet backgrounds, the W originating from the top quark is required to have decayed leptonically. We demand therefore a high-energy electron or muon ($E_T(e) > 20$ GeV, or $P_T(\mu) > 20$ GeV/ c) and large missing energy from the undetected neutrino $\cancel{E}_T > 25$ GeV (using jets corrected to the hadron level). We reject dilepton events from $t\bar{t}$ and Z decays, by requiring the dilepton mass to be outside the range: 76 GeV/ $c^2 < M_{\ell\ell} < 106$ GeV/ c^2 . The backgrounds surviving these selections can be classified as “non-top” and $t\bar{t}$. The non-top backgrounds are: $Wb\bar{b}$, $Wc\bar{c}$, Wc , mistags (light quarks misidentified as heavy flavor jets), non- W (events where a jet is erroneously identified as a lepton), and diboson WW , WZ , and ZZ . We remove a large fraction of the non-top and $t\bar{t}$ backgrounds by demanding exactly two “tight” jets with $E_T > 20$ GeV (corrected to hadron level) and $|\eta| < 2.8$ be present in the event. At least one of the two tight jets should be tagged as a b -quark jet by using displaced vertex information from the silicon vertex detector (SVX). The non- W content of the selected dataset is further reduced by imposing a set of requirements on *i*) transverse mass of the reconstructed W boson, *ii*) the \cancel{E}_T significance (electron events only), and *iii*) the angle between the \cancel{E}_T vector and the transverse momentum vector of the leading jets (electron events only).

Process	2-jet Prediction
t -chan	37.0
s -chan	23.9
$t\bar{t}$	85.3
$Wb\bar{b}$	319.6
$Wc(c)$	324.2
W +LF	214.6
Z +jets	13.8
<i>Diboson</i> (WW, WZ, ZZ)	40.7
non- W	44.5
Total predicted	1103.7
Observed	1078

TABLE I: Background estimates used in this analysis, along with the observed total (last row). The systematic uncertainties on these predictions, as used in the interpretation of the results, are given in Table II.

III. SIGNAL AND BACKGROUND ESTIMATIONS

Depending on the method by which their contributions are estimated, the different processes can be classified into two categories: Monte Carlo-based or data-based estimations. For example, the $t\bar{t}$, diboson (WW , WZ and ZZ) contributions, and $Z \rightarrow \ell\ell$ belong to the first category. The same can be said about signal estimations. For all these processes, the contributions are estimated using a combination of Monte Carlo-generated samples (to extract acceptance and efficiency factors) and the theoretical cross sections (to normalize the rates).

The other category contains those background processes whose estimations require the use of CDF data: W +heavy flavor ($Wb\bar{b}$, $Wc\bar{c}$, Wc), mistags, and non- W events. Their contributions are obtained using a similar method with that employed in Ref [4], with a few differences. One difference is the larger η range for the jet definition ($|\eta| < 2.8$) used in this search. The other difference is that a scale factor for the heavy flavor fraction is used. This was calculated using tagged W + 1 jet data, and was found to be 1.4 ± 0.4 .

The expected and observed event yields corresponding to the 1.5 fb^{-1} dataset are given in Table I, for both Monte Carlo based and data based background estimates.

IV. SPECIAL EVENT VARIABLES

A. ANN extended B -tagger

An Artificial Neural Network (ANN) [5] was developed to increase the b -quark purity of the sample selected by the standard b -tagging algorithm. The latter is based on measuring displaced (secondary) vertices, and in addition to b -jets it also selects a significant fraction of c - and light flavor jets (as much as 50%). The extended (ANN) tagger is applied to jets selected by the standard b -tagger, and exploits mainly the long lifetime (1.6 ps) of b -hadrons. Other features used by the ANN are the high b -quark mass, the high decay multiplicity, and the decay into leptons. For illustration, Fig. 2 shows good shape agreement between the ANN output distributions for the W + 2 jet data and a sum of the individual background components normalized to data.

B. Kinematic Solver

We can use the measured momenta of the final state particles to reconstruct the W boson and the top quark, and constrain the reconstructed masses $M_{\ell\nu}$ and $M_{\ell\nu b}$ to 80.4 GeV and 175 GeV, respectively. The constraint of the event kinematics to these known masses improves the reconstruction of signal events, worsens the reconstruction of background events, and aids in the separation of the single-top signal from the background. The widths of the top quark and W boson mass distributions at the parton level are of the order of 2 GeV. At reconstructed level the measurement uncertainties are much larger, of the order of 20-40 GeV for $M_{\ell\nu b}$, if one were to use the reconstructed values in the t and s channels, respectively.

The kinematic constraints' use is twofold. First, the χ^2 , which is constructed out of the difference between the *measured* jet energies, angles and \cancel{E}_T and those required by the kinematic constraints, can be used instead of the reconstructed $M_{\ell\nu b}$ as a variable which helps separate signals from backgrounds. The second use of the kinematic

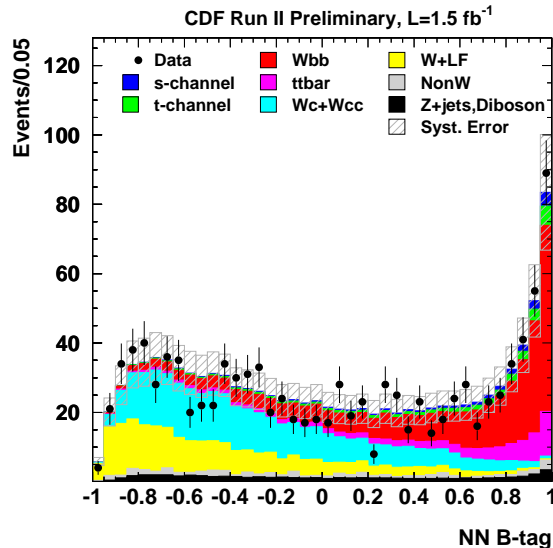


FIG. 2: The ANN tagger output distributions for the CDF $W+2$ jets events (points) compared to the Monte Carlo expectations.

constraints is to ensure that the input to the matrix element calculation has four-vectors which correspond to on-shell W bosons and top quarks.

An inventory of the constraints used is as follows:

- The lepton momentum vector is constrained to its measured value.
- The p_T of the top quark is constrained to its measured value.
- The direction and mass of the b jet from top decay are constrained to their measured values.
- $M_{\ell\nu}$ is constrained to 80.4 GeV, resulting in a second-degree equation with two neutrino p_z solutions.
- $M_{\ell\nu b}$ is constrained to 175 GeV.

These constraints are sufficient to solve for the energy of the b jet from top decay, with no regard to its measured value. The ambiguity choices – two possible assignments of the b -jet from top decay, and two neutrino p_z solutions (usually), means that the kinematic interpretation must be done four times.

The output from the kinematic solver is a set of neutrino and b -jet four-vector solutions, which are used to reconstruct kinematic variables. Also provided is the χ^2 output mentioned above, which indicates how far from the measured values of the b -jet energy and the \cancel{E}_T the solver found its solutions. If the wrong choice of b -jet from top is made, then the χ^2 is typically worse than if the correct choice is made, and thus the χ^2 variable can be used to select the b jet in events in which the choice is ambiguous. The χ^2 definition is

$$\chi^2 = \frac{(E_b^{\text{solved}} - E_b^{\text{meas}})^2}{\sigma_b^2} + \frac{(M_{\ell\nu b} - 175\text{GeV})^2}{\sigma_{m_t}^2} + \frac{(\Delta \cancel{E}_T)^2}{\sigma_{\cancel{E}_T}^2}, \quad (1)$$

where σ_b is taken to be 9 GeV, σ_{m_t} is taken to be 1 GeV, and $\sigma_{\cancel{E}_T}$ is taken to be 11 GeV.

V. LIKELIHOOD FUNCTION TECHNIQUE

No single variable encodes all conceivable signal-background separation, and so a likelihood function [6] is proposed to combine several variables together into a discriminant which can be used to compute limits or to discover a signal.

The likelihood function \mathcal{L} is constructed by first forming histograms of each variable (n_i bins per variable), separately for the signal distributions and for several background distributions, denoted $f_{i,jk}$ for bin j of variable i for the event

class k . For the signal, $k = 1$, and in this note, four background classes are considered: $Wb\bar{b}$, $t\bar{t}$, $Wc\bar{c}/Wc$, and mistags, which are event classes 2, 3, 4 and 5. These histograms are normalized such that $\sum_{j=1}^{n_i} f_{ijk} = 1$ for all i and all k . The likelihood function for an event is computed by evaluating in which bin j_i in which the event falls in the distribution of variable i , and computing

$$p_{ik} = \frac{f_{ij_i k}}{\sum_{m=1}^5 f_{ij_i m}}, \quad (2)$$

which is used to compute

$$\mathcal{L}_k(\{x_i\}) = \frac{\prod_{i=1}^{n_{\text{var}}} p_{ik}}{\sum_{m=1}^5 \prod_{i=1}^{n_{\text{var}}} p_{im}}. \quad (3)$$

The signal likelihood function is the one which corresponds to the signal class of events, \mathcal{L}_1 .

Two likelihood functions are computed – \mathcal{L}_t using the t -channel single-top signal in the signal reference histograms, and \mathcal{L}_s using the s -channel single-top signal in the signal reference histograms. Plots of all input variables can be found on the Likelihood Function search public page [15].

A. t -channel Likelihood Function.

The t -channel likelihood function, \mathcal{L}_t , uses seven variables, and assumes the b -tagged jet comes from top decay. For doubly-tagged events, we set $\mathcal{L}_t = 0.001$. The t -channel likelihood function uses the following seven variables:

- H_T , the scalar sum of the transverse energies of the two tight jets, the lepton, and the missing transverse energy.
- $Q \times \eta$, the charge of the lepton times the pseudorapidity of the tight jet which is not b -tagged.
- χ_t^2 , output from the kinematic solver for the t -channel combination described above.
- $\cos \theta_{t\text{-chan}}$, the cosine of the angle between the lepton and the untagged tight jet in the top decay frame.
- M_{jj} , the invariant mass of the two tight jets.
- $\log(\text{ME}_{t\text{-chan}})$, the logarithm of the MADGRAPH matrix element computed using the constrained four-vectors of the b , the ℓ and the ν .
- ANN b -tag output.

We show the \mathcal{L}_t likelihood function resulting from combining the above seven variables in Fig. 3. A good signal-background separation is apparent.

B. s -channel Likelihood Function.

The s -channel likelihood function, \mathcal{L}_s , uses eight variables and is constructed in the same way as the t -channel likelihood. A b -choosing algorithm optimized for s -channel two-jet bin is used to choose the b -jet from top decay in the s -channel likelihood function. For this algorithm, the following variable is constructed:

$$c_{s2} = Q * (\eta_1 - \eta_2) - (\chi_{min,1}^2 - \chi_{min,2}^2)/5, \quad (4)$$

Here Q is the charge of the lepton, η_i is the jet pseudorapidity, and $\chi_{min,i}^2$ is the smaller of the two kinematic-solver χ^2 values, choosing jet i as the b from top decay, and considering both $p_{z,\nu}$ solutions. If $c_{s2} > 0$ then jet 1 is assigned to be the b from top decay, and if $c_{s2} < 0$, then jet 2 is assigned to be the b from top decay. The correct b assignment fraction in 2-jet s -channel signal Monte Carlo events is 81%. The smaller of the two $p_{z,\nu}$ solutions is taken for the neutrino, and the correct assignment fraction is 75%, including events in which both $p_{z,\nu}$ solutions are the same.

The input variables to the s -channel likelihood function are

- χ_s^2 , the output of the kinematic solver for the choice of b -jet optimized for the s -channel likelihood.
- $E_T(j1)$, the transverse energy of the leading jet.

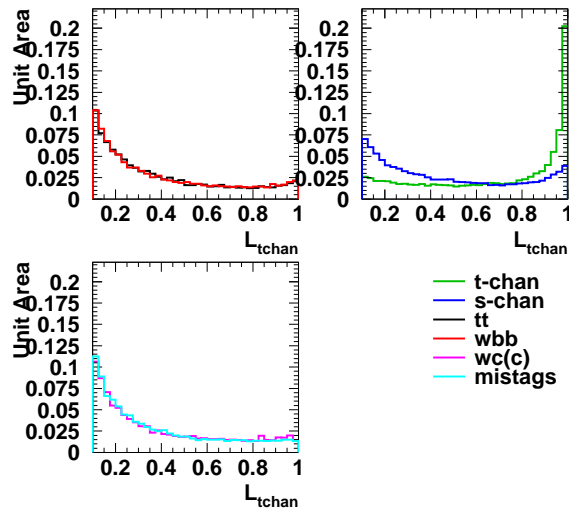


FIG. 3: The distributions of the t -channel likelihood function \mathcal{L}_t normalized to unit area.

- $\text{ME}_{t\text{-chan}}$, the MADGRAPH matrix element computed using the constrained four-vectors of the b , the ℓ and the ν , assuming t -channel signal production.
- $\text{ME}_{s\text{-chan}}$, the MADGRAPH matrix element computed using the constrained four-vectors of the b , the ℓ and the ν , assuming s -channel signal production, using the s -channel choice of b -jet.
- H_T , the scalar sum of the transverse energies of the two tight jets, the lepton, and the missing transverse energy.
- $\log(M_{\ell\nu b}^s \times H_T)$, the product of the s -channel optimized $M_{\ell\nu b}$ and H_T , using the s -channel choice of b -jet.
- ANN b-tag output
- $M_{\ell\nu jj}$, the invariant mass of the lepton, neutrino, and two tight jet system.

VI. SYSTEMATIC UNCERTAINTIES

Systematic variations in the rates and shapes of the likelihood distributions are considered for the signals and backgrounds in the sample. Systematic uncertainties contributing to the shape uncertainties are the jet energy scale (JES), initial state radiation (ISR) and final state radiation (FSR) variations, variations in the NN b-tag output distributions, variations in the flavor composition of the non- W sample, and variation in the Q^2 scale in ALPGEN. These same uncertainties contribute to the rate uncertainties, and additional contributions come from the uncertainty in the integrated luminosity, the parton distribution function used, the b-tag scale factor, the $t\bar{t}$ cross section prediction, and uncertainties propagated from the data-based background estimates. Table II enumerates the relative rate errors on the backgrounds used in the limit calculations, and also indicates which sources of systematic error have shape errors associated with them which are used in the p -value calculation and limit setting.

VII. RESULTS

We use the likelihood functions described above to search for single-top quark production. The degree to which we have evidence for single-top production is denoted by a p -value, which is the probability of observing data at least as signal-like as what we observed.

Source name	s-chan signal	t-chan signal	Wbb	$Wc\bar{c}$	$t\bar{t}$	Mistags	nonW	Diboson Z+jets
LUMI	0.06	0.06	0	0	0.06	0	0	0.06
BTAG	0.042	0.042	0	0	0.042	0	0	0.042
NNBTAG	*	*	*	*	*	*	0	0
ISR	+0.032 -0.01	+0.032 -0.01	0	0	0	0	0	0
FSR	+0.053 -0.015	+0.053 -0.015	0	0	0	0	0	0
PDF	+0.01 -0.01	+0.011 -0.017	0	0	0.024	0	0	0
JES	+0.003* -0.008	-0.008* +0.004	-0.076* +0.070	-0.058* +0.065	-0.091* +0.098	0	0	+0.015* -0.032
WJETS	0	0	0.35	0.35	0	0	0	0
DIBOSON	0	0	0	0	0	0	0	0.13
MISTAG	0	0	0	0	0	0.14	0	0
NONW	0	0	0	0	0	0	0.6	0
NONWFLAV	0	0	0	0	0	0	*	0
NonWType	0	0	0	0	0	0	*	0
TTBAR	0	0	0	0	0.21	0	0	0
QSQUARED	0	0	*	*	0	0	0	0
DRJJ	*	*	*	*	*	*	*	*
PHXE	*	*	*	*	*	*	*	*
ETAJ2	*	*	*	*	*	*	*	*

TABLE II: Fractional (relative) rate uncertainties on the components expected to contribute to the two-jet bin's contents. Uncertainties are symmetric unless positive and negative uncertainties are listed. The uncertainties are listed as up, down pairs, ie JESup or ISRup or JESdown or ISRdown . A “*” indicates that a shape error is estimated for this nuisance parameter on that component of the expectation

The data are also used to measure the single-top production cross section. Two fits are performed. The first fit assumes the Standard Model ratio of σ_s/σ_t , while the other explores the two-dimensional plane (σ_s, σ_t) . Maximum-likelihood techniques are used in both cases.

A frequentist approach (except in the handling of the systematic uncertainties) is used to determine the p -value for single-top production. For 1-D p -value calculation only the 40-bin distribution of \mathcal{L}_t , has been used. The data are compared with two hypotheses. The null hypothesis, H_0 , assumes Standard Model processes except single-top quark production, while the test hypothesis, H_1 , assumes all Standard Model processes including single-top quark production. The likelihood ratio is defined as:

$$-2 \ln Q = -2 \ln \frac{p(\text{data}|H_1, \hat{\theta})}{p(\text{data}|H_0, \hat{\hat{\theta}})}, \quad (5)$$

where θ are the nuisance parameters describing the uncertain values of the quantities studied for systematic error, $\hat{\theta}$ are the best-fit values of θ under H_1 , and $\hat{\hat{\theta}}$ are the best-fit values of the nuisance parameters under H_0 . Two sets of pseudoexperiments are performed, one assuming H_1 and the other assuming H_0 . On each pseudoexperiment, the values of the nuisance parameters are chosen randomly based on the errors given in Table II. The distributions of the values of $-2 \ln Q$ are shown in Figure 5 for both hypotheses, and for the data.

The p -value is the probability that $-2 \ln Q < -2 \ln Q_{\text{obs}}$, assuming the null hypothesis H_0 . The p -value was found to be 3.1×10^{-3} , which corresponds to a 2.7σ excess. The sensitivity of the analysis is computed as the median expected p -value assuming a signal is truly present. The median $-2 \ln Q$ is extracted from the H_1 distribution, and the integral of the H_0 distribution of $-2 \ln Q$ to the left of this median value is the median expected p -value. The value thus obtained is 2.0×10^{-3} , corresponding to 2.9σ .

In order to measure the single-top production cross section, a one-dimensional fit is performed to the t -channel likelihood output histogram. The Standard Model ratio between σ_s and σ_t and a flat prior in $\sigma_s + \sigma_t$ is assumed. The nuisance parameters are integrated over (“marginalized”) as described in [11],[7]. The distribution of the posterior is shown in Figure 6. The maximum of the posterior is taken to be the best-fit value, and the 68% confidence interval is taken to be the shortest interval containing 68% of the integral of the posterior distribution. The resulting fit is $\sigma_s + \sigma_t = 2.7_{-1.1}^{+1.3}$ pb.

We also test models in which σ_s and σ_t may not be in their Standard Model ratio. In this case, the t -channel and s -channel likelihood functions (\mathcal{L}_s and \mathcal{L}_t) are used to explore the two-dimensional plane (σ_s, σ_t) . The value of $-2 \ln \mathcal{L}$ is computed at each value of (σ_s, σ_t) , and at each test hypothesis point, the values of the nuisance parameters are chosen to minimize $-2 \ln \mathcal{L}$. The minimum of $-2 \ln \mathcal{L}$ over the (σ_s, σ_t) plane occurs at (1.1,1.3) pb. These results

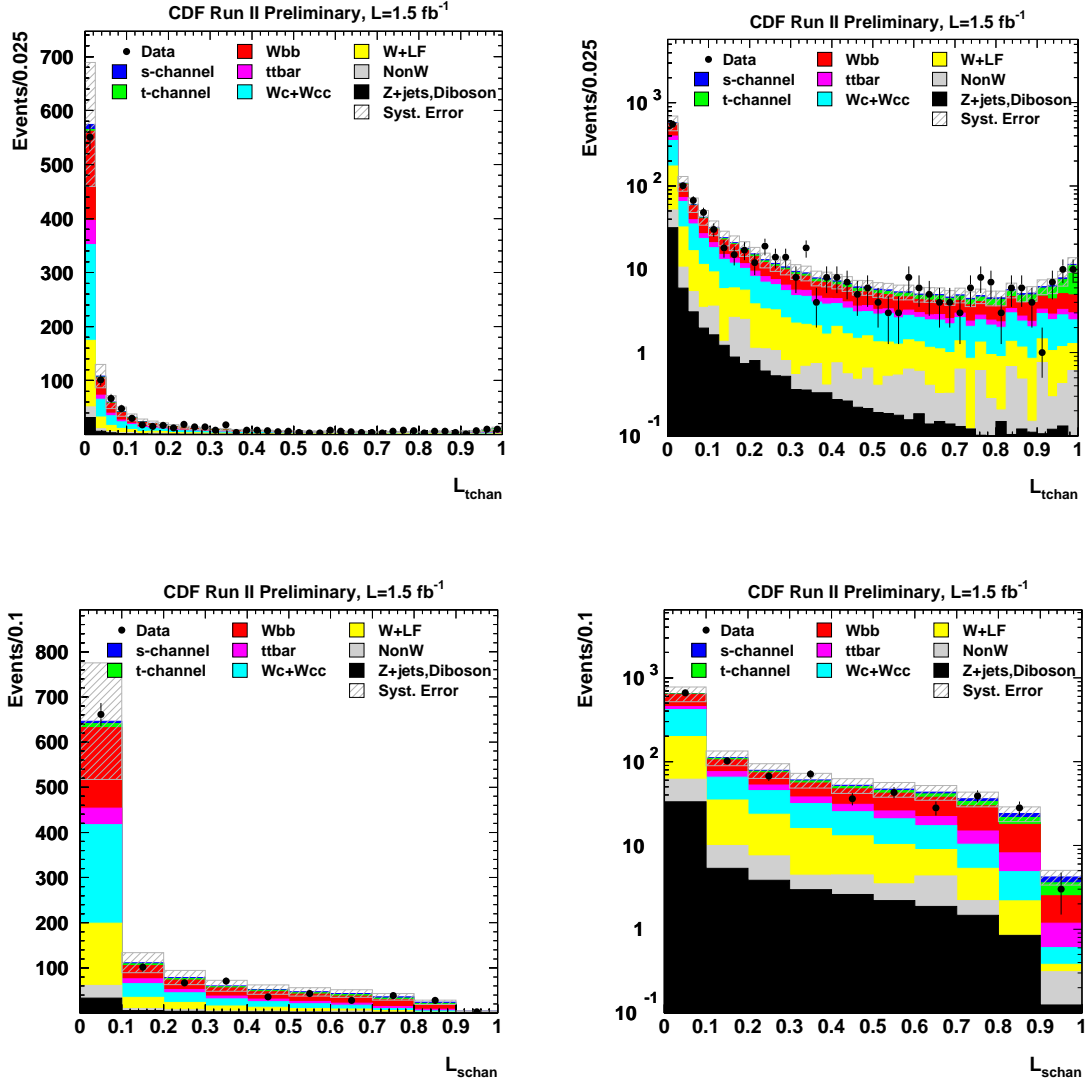


FIG. 4: The distributions of the t -channel (upper) and s -channel (lower) likelihood functions for CDF data compared to the Monte Carlo distributions normalized to the expected contributions. The Monte Carlo contributions are multiplied by 1.1 to match the data normalization. A linear (logarithmic) scale is used for the left (right) plots.

are shown in Figure 7, along with predictions [12] of σ_t and σ_s of additional models including top-flavor, FCNC's, a fourth generation model, and a top-pion model and the SM prediction and its uncertainty. Using the full range of the 1σ error contour as the errors on the separate measurements, we obtain $\sigma_s = 1.1^{+1.4}_{-1.1}$ pb and $\sigma_t = 1.3^{+1.2}_{-1.0}$ pb.

Finally, the maximum-likelihood analysis can be used to extract an upper limit on the production cross section at the 95% confidence level. The interpretation assuming the Standard Model ratio of σ_s/σ_t is used here. Using the Bayesian procedure of integrating the posterior density distribution with respect to the cross section from σ_{95} to infinity, we obtain an upper limit on the single-top production cross section of 5.1 pb. In the absence of single-top production cross section, a median expected limit of 2.1 pb is expected. If the σ_s/σ_t ratio assumption is relaxed, then the contours shown in Figure 7 may be used.

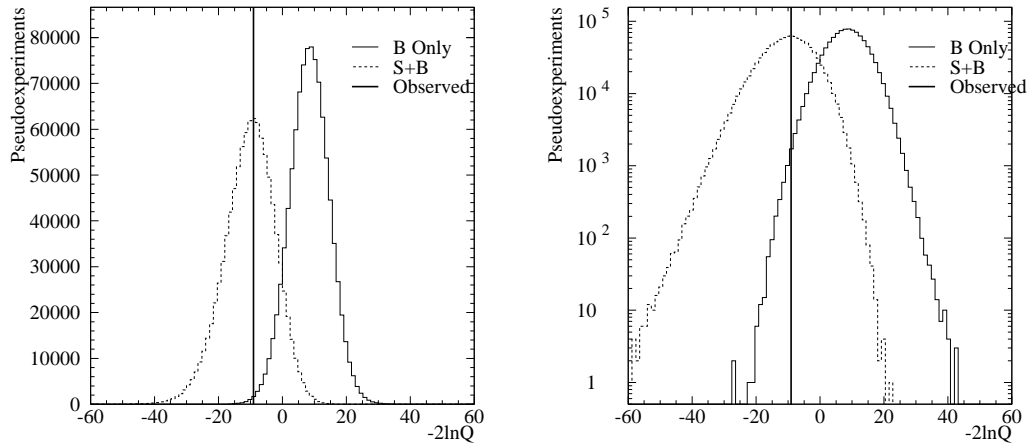


FIG. 5: Distributions of $-2\ln Q$ for the test hypothesis, H_1 , which assumes Standard Model backgrounds plus Standard-Model single-top production (dashed histograms), and for the null hypothesis, H_0 , which assumes single-top production is absent (solid histograms). The observed value of $-2\ln Q$ is indicated with a solid, vertical line. The top plot has a linear scale and the bottom plot is the same on a logarithmic scale. The p -value is the fraction of the integral of the H_0 curve to the left of the data.

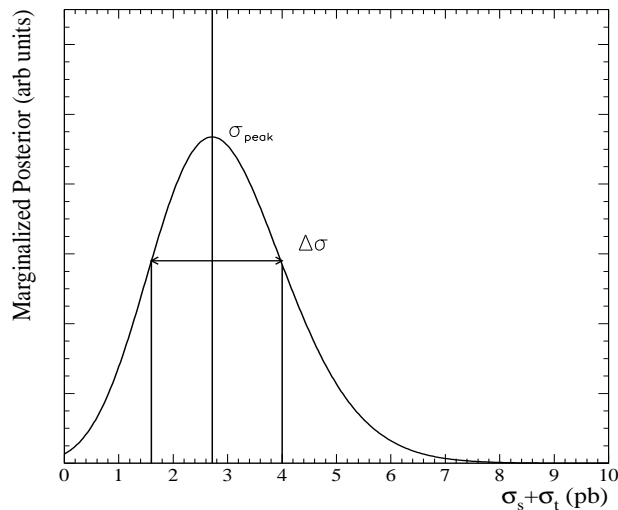


FIG. 6: Fit for $\sigma_s + \sigma_t$. A uniform prior in $\sigma_s + \sigma_t$ is assumed, and the SM ratio of σ_s/σ_t is also assumed. The Bayesian posterior, marginalized over nuisance parameters, is shown. The maximum value is the central value of the cross-section fit, and the smallest interval enclosing 68% of the integral of the posterior is the quoted interval. The measured result is $\sigma_s + \sigma_t = 2.7_{-1.1}^{+1.3}$ pb.

VIII. CONCLUSION

We present an analysis of the 1.5 fb^{-1} dataset in search of single-top-quark events, using a multivariate likelihood function technique, with a likelihood function designed to isolate t -channel signal events, and a separate likelihood function designed to isolate s -channel signal events. We find an observed p -value of 3.1×10^{-3} , which corresponds to a 2.7σ excess over the Standard Model backgrounds. The median expected p -value assuming single-top production occurs at the Standard Model rate, is 2.0×10^{-3} , corresponding to 2.9σ .

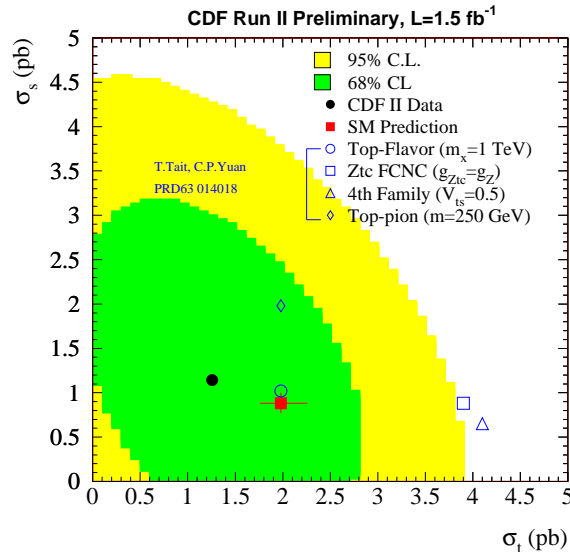


FIG. 7: The best fit value for σ_s and σ_t obtained from fitting the 2-dimensional \mathcal{L}_s vs. \mathcal{L}_t distribution. A $\Delta\chi^2$ is computed, comparing the $\chi^2(\sigma_s, \sigma_t)$ against that of best-fit corresponding to $(\sigma_s, \sigma_t) = (0.1 \text{ pb}, 0.2 \text{ pb})$. The 1σ fit region and the region allowed at the 95% C.L. are shown, along with the Standard Model prediction.

The analysis proceeds on to a measurement of the single-top production cross section, assuming that the branching ratio $B(t \rightarrow Wb) \approx 100\%$, and that $M_t = 175 \text{ GeV}$. Assuming further that the s -channel and t -channel cross sections obey their Standard Model theoretically predicted ratio, the single-top cross section is measured to be $\sigma_s + \sigma_t = 2.7_{-1.1}^{+1.3} \text{ pb}$. The Standard Model prediction for $\sigma_s + \sigma_t$ is $2.86_{-0.33}^{+0.40} \text{ pb}$ [3] (The theory errors on σ_s and σ_t have been added linearly here, assuming they are 100% correlated).

Models are tested allowing arbitrary σ_s and σ_t , and 68% and 95% confidence contours are shown in Figure 7. The fit values are $\sigma_s = 1.1_{-1.1}^{+1.4} \text{ pb}$ and $\sigma_t = 1.3_{-1.0}^{+1.2} \text{ pb}$.

Acknowledgments

We thank the Fermilab staff and the technical staffs of the participating institutions for their vital contributions. This work was supported by the U.S. Department of Energy and National Science Foundation; the Italian Istituto Nazionale di Fisica Nucleare; the Ministry of Education, Culture, Sports, Science and Technology of Japan; the Natural Sciences and Engineering Research Council of Canada; the National Science Council of the Republic of China; the Swiss National Science Foundation; the A.P. Sloan Foundation; the Bundesministerium für Bildung und Forschung, Germany; the Korean Science and Engineering Foundation and the Korean Research Foundation; the Science and Technology Facilities Council and the Royal Society, UK; the Institut National de Physique Nucleaire et Physique des Particules/CNRS; the Russian Foundation for Basic Research; the Comisión Interministerial de Ciencia y Tecnología, Spain; the European Community's Human Potential Programme; the Slovak R&D Agency; and the Academy of Finland.

-
- [1] D. Acosta *et al.* (CDF Collaboration), Phys. Rev. D **65**, 091102 (2002); D. Acosta *et al.* (CDF Collaboration), Phys. Rev. D **69**, 052003 (2004); D. Acosta *et al.* (CDF Collaboration), Phys. Rev. D **71**, 012005 (2005).
[2] B. Abbott *et al.* (DØ Collaboration), Phys. Rev. D **63**, 031101 (2001); V. M. Abazov *et al.* (DØ Collaboration), Phys. Lett. B **517**, 282 (2001); V. M. Abazov *et al.* (DØ Collaboration), Phys. Lett. B **622**, 265 (2005).
[3] B. W. Harris *et al.*, Phys. Rev. D **66**, 054024 (2002); Z. Sullivan, Phys. Rev. D **70**, 114012 (2004).

- [4] The CDF Collaboration, “Measurement of the Top Pair Production Cross Section in the Lepton+Jets Decay Channel” CDF Note 8795, 2007 (*public*)
- [5] T. Chwalek *et al.*, “Update of the Neural Network b Tagger for Single-Top Analyses”, CDF note 8903, 2007 (*internal*).
- [6] R. Barlow, “Statistics: a Guide to the Use of Statistics in the Physical Sciences” John Wiley and Sons, LTD, West Sussex, England (1989).
- [7] T. Junk, “Sensitivity, Exclusion and Discovery with Small Signals, Large Backgrounds, and Large Systematics”, CDF note 8128 (*internal*). Also see: A. L. Read, J. Phys. G: Nucl. Part. Phys. **28**, 2693 (2002); P. Bock *et al.* (the LEP Collaborations), CERN-EP-98-046 (1998) and CERN-EP-2000-055 (2000).
- [8] M. Feindt, e-Print Archive physics/0402093 (2004).
- [9] T. Tait and C. P. Yuan, Phys.Rev. **D63** (2001) 014018, available online as arXiv:hep-ph/0007298 (2000).
- [10] Luc Demortier, Louis Lyons, Joel Heinrich, Giovanni Punzi, John Conway, Craig Blocker, Tom Junk, CDF Note 8023 (2006) (*internal*).
- [11] J. Heinrich, “Bayesian limit software: multi-channel with correlated backgrounds and efficiencies”, CDF note no. 7587 (*internal*).
- [12] T. Tait and C. P. Yuan, Phys.Rev. **D63** (2001) 014018, available online as arXiv:hep-ph/0007298 (2000).
- [13] V. M. Abazov *et al.* [D0 Collaboration], Phys. Rev. Lett. **98**, 181802 (2007) [arXiv:hep-ex/0612052];
also see: http://www-d0.fnal.gov/Run2Physics/top/top_public_web_pages/top_public.html
- [14] M. Buehler *et al.*, “Search for Electroweak Single-Top-Quark Production using Neural Networks with 955 pb-1 of CDF”, CDF Note 8677, 2007 (*public*);
S. Budd *et al.*, “Search for Single-Top-Quark Production Using a Multivariate Likelihood Technique”, CDF Note 8585, 2007 (*public*);
F. Canelliet *al.*, “Search for Single-Top-Quark Production in 955 pb-1 using the Matrix Element Technique”, CDF Note 8588, 2007 (*public*)
also see: <http://www-cdf.fnal.gov/physics/new/top/top.html>
- [15] see: http://www-cdf.fnal.gov/physics/new/top/2007/singletop/LF1_5fb/LF1_5fb_Public_page.html